1

A vortex subjected to a shear: an experimental study

By O. PAIREAU[1], P. TABELING[1] and B. LEGRAS[2]

[1] Laboratoire de Physique Statistique,

[2] Laboratoire de Météorologie Dynamique,
Ecole Normale Supérieure, 24 rue Lhomond, F-75231 Paris Cedex 05, France

The two-dimensional erosion of a vortex subjected to an external, adverse shear is studied experimentally. The flow takes place in a thin stratified layer; the vortex is produced by electromagnetic forcing, whereas the shear is driven mechanically. The system thus allows the vortex strength and the external shear to be controlled independently. We observe the so-called 'erosion' process, i.e. the progressive decrease of the vortex area, leaving the vortex core unaffected. This process is controlled by the ratio $\gamma = S/\omega_{max}$, where ω_{max} and S are respectively the maximum vorticity of the vortex and the external shear. At small γ, the erosion is weak and the vortex survives over the duration of the experiment. At large γ, the vortex is first eroded, and then, after a critical time, becomes stretched and eventually breaks up into filaments. During the first period of time, the compensated maximum vorticity (with friction decay removed) is constant and the vortex area decreases, while beyond the critical time, both quantities decrease with time. A critical value for γ, defining the transition between these two regimes, is determined experimentally: $\gamma_c = 0.051 \pm 0.017$. The breaking process itself, during which the vorticity of the vortex core decreases, is investigated. All the qualitative aspects of the erosion process, the onset of breaking and the breaking process itself are found to be in excellent agreement with the theoretical and numerical description. The experimental value of γ_c and the properties of the filamentation process are consistent with the numerical estimates.

1. Introduction

The deformation of two-dimensional vortices under the action of an external velocity field caused by other vortices or a large-scale flow plays a crucial role in two-dimensional turbulence and geophysical fluid dynamics. It is found empirically that either such vortices are elongated and then return to their initial shape or they undergo irreversible deformations, leading to the generation of vorticity filaments expelled from the vortex into the background field. Filamentation accompanies total or partial merging of two vortices, a phenomenon which has received considerable attention in the literature, but is mostly observed in the absence of merging under the action of a large-scale strain. The importance of these phenomenon in the middle atmosphere is well illustrated in Waugh *et al.* (1994). As an idealized case of maximum simplification, the dynamics of an isolated patch of uniform vorticity submitted to a strain was first studied by Moore & Saffman (1971) and Kida (1981). Kida showed that, in the presence of an external shear, an elliptical patch can be stationary if the shear is not too large. In particular, Kida derived an exact solution of the problem, in the form of an elliptical vorticity patch undergoing regular oscillations. Later, Dritschel (1990)

showed that some of these solutions are unstable to perturbations developing on the boundary of the vortex.

Recently, Legras & Dritschel (1993, 1994) studied the behaviour of an initially axisymmetric distributed vortex subjected to an external adverse shear, i.e. one which opposes the rotation of the vortex. They showed that, unlike the uniform patch, stripping develops as a direct response to the shear and not as a linear instability. Stripping erodes the external vorticity layers which are expelled as filaments while the interior layers retain quasi-elliptical shapes. A particularly interesting result is that vortex breaking is controlled by a critical value γ_c of the ratio between the shear and the maximum vorticity, practically independently of the vorticity profile of the vortex, provided that it is smooth, and of the Reynolds number of the flow. In a more general deformation field (pure shear corresponds to the particular case in which strain equals rotation), the critical value depends on an additional parameter – the ratio between rotation and strain. The influence of viscosity was studied by Mariotti, Legras & Dritschel (1994), in the case of pure shear; they showed that diffusion first induces a continuous, slow erosion of the vortex, and then, after some critical time, the vortex becomes stretched and eventually breaks up. In this problem, the role of viscosity is thus somehow counter-intuitive since it favours the break-up of the vortex. An interesting property found by Mariotti *et al.* (1994) is that the critical value γ_c for the onset of vortex break-up is almost independent of viscosity, provided that the Reynolds number is large enough. All these results are based on numerical and analytical calculations but in the literature there is no experimental study of the effect of shear on an isolated vortex, despite its importance in two-dimensional flows. Let us mention here the experiments of Trieling (1996) which address the problem of two-dimensional vortices in a strain flow. This situation contrasts with numerous studies on merging and dipole collisions (e.g. Griffiths & Hopfinger 1986; van Heijst & Flor 1989; Voropayev & Afanasyev 1991).

In this paper, we report an experimental study of a vortex subjected to an adverse shear flow in which we perform a qualitative and quantitative comparison between experiment and theory. The design of this experiment is such that the flow develops in a quasi-two-dimensional configuration, and that we independently control the vortex strength and the external shear. The paper is organized as follows: §2 presents the experimental set-up; §3 describes the experimental observations; and §4 compares them with numerical predictions, offers some discussion and proposes a conclusion.

2. Experimental set-up

2.1. *Description of the experiment*

The experimental system is schematically represented in figure 1. The cell is 40 cm long, 25 cm wide and 5 cm high, and it is filled with two layers of salty water, 6 mm thick for the lower layer and 2 mm for the upper layer. The concentration of the lower layer is twice that of the upper layer. The flow thus takes place in a stably stratified fluid. The stratification tends to inhibit the vertical motions and thus to reduce the three-dimensional effects, in particular within the upper layer. To produce the external shear flow, we use two co-rotating disks, 15 cm in diameter and 5.5 mm thick, driven by DC motors, and immersed in the lower layer. This configuration minimizes the mixing of the two layers (if both layers were driven together, Ekman pumping would tend to mix them). As the upper and lower layers are coupled, the shear created occurs in both layers. The distance d between the disks is 4 cm. In such a geometry, the streamlines of the external velocity field are almost parallel in the region between the disks. The
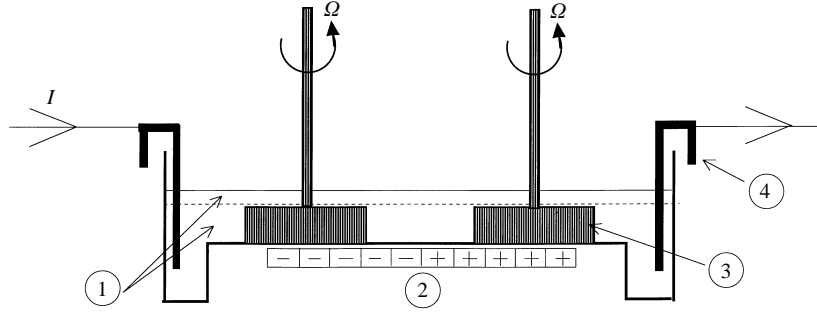
FIGURE 1. Schematic representation of the experimental system. 1: Two layers of salty water (thickness: 6 and 2 mm). The density of the lower and upper layers are respectively equal to 1.155 kg l^{-1} and 1.072 kg l^{-1}. 2: Permanent magnets. 3: Co-rotating disks. 4: Electrodes.

vortex is produced in this region by electromagnetic forcing, using a method which has been described in several references (e.g. Tabeling *et al*. 1991; Dolzhanskii, Krymov & Manin 1992). In our case, an electric current is driven horizontally from one side of the cell to the other (figure 1), with typical intensity $I = 1.5$ A. Permanent magnets are located just below the fluid, each of them producing a magnetic field of maximum intensity 0.32 T. The interaction of the magnetic field with the electric current produces a Lorentz force defined by $F = h \times B$, where j is the current density and B is the magnetic field. In the case of a suddenly applied current (which corresponds to our experimental situation), the short-time response of the flow is governed by

$$\frac{\partial \boldsymbol{\omega}}{\partial t} = \text{curl}\,(\boldsymbol{j} \times \boldsymbol{B}), \qquad (2.1)$$

where $\boldsymbol{\omega}$ is the vorticity. For a horizontal homogeneous current density $\boldsymbol{j}$, the vertical vorticity ω_z is thus

$$\omega_z \approx j \frac{\partial B_z}{\partial x} t, \qquad (2.2)$$

where the direction x is that of the electric current. In other words, the vertical vorticity is proportional to the gradient of the vertical magnetic field along the electric current. In the experimental set-up, we use a line of permanent magnets, located just below the cell, to produce a single vortex. This line is divided into two halves with opposite polarization. In each half-line, all the magnets have their north pole in the same direction. We shall characterize below, in some detail, the structure of this vortex. The upper layer flow is visualized by floating latex particles of 10 μm size. Images of the flow are taken from a video camera located above the experimental cell, and recorded on a U-matic video tape recorder. During the recording, an audio signal is generated by the computer and recorded on the sound channel of the video tape recorder, so as to identify each frame of the video signal. In a second step, the video frames are digitized and stored on a magneto-optical disk. The calculations are performed on a Macintosh IIfx computer, assisted by a double Digital Signal Processor board DSP32C. The method of velocity retrieval (Cardoso, Marteau & Tabeling 1994) consists in discretizing the surface flow on a square grid, usually with 40×40 points, and in computing for each node an average velocity within a box of $l \times l$ pixels centred on the node. This is obtained by calculating the spatial correlation of two images of the cell separated by a time interval δt. The position of maximum correlation provides the local displacement of the particles, giving an average velocity with a spatial resolution

of the size of the cell. The choice of the size l – typically $l = 32$ pixels of the elementary box – is guided by the following considerations.

(a) l is much smaller than a typical scale of variation of the flow.

(b) Each box contains several particles, so as to take advantage of statistical averaging. In practice, five particles per box is a minimal value.

(c) Most of the particles stay within the box during the time interval δt. This introduces some limitations on the largest measurable velocity.

The choice of δt also requires some care: for a given box size, it must satisfy condition (c), and must be such that the displacement of the particles is measurable. We took $\delta t = 0.04$ s. Even when all the above criteria are met, we may obtain, in some cells, aberrant data (typically one per thousand). To check the validity of the measurement, we compute a local divergence of the velocity field by finite difference around every suspicious point. When this value exceeds some threshold, we replace the computed velocity by a local average of the neighbouring values.

The calculation of the vorticity field is then done by polynomial interpolation within a moving window followed by numerical differentiation. The accuracy of the measurement of the velocity field can be estimated to a few percent, and that of the vorticity to about 10 %. Also, an estimation of the divergence yields that of the vertical motions, i.e. the three-dimensional effects, by continuity. It turns out that the divergence is less than 10 % of the maximum vorticity in all experiments. This indicates that the vertical velocity is much weaker than the horizontal motion.

The determination of the experimental protocol is an important issue. In all the experiments, we use the following procedure in sequence:

(i) the disks are rotated at constant speed until the flow is fully established (this takes a few minutes);

(ii) an electric current I is imposed for a prescribed short period of time τ;

(iii) the current is quenched at a time which is subsequently taken as the origin $t = 0$;

(iv) the decay process is recorded; vortex erosion is studied during this phase (which takes typically 20 s).

Throughout phases (ii)–(iv) the disks are maintained at constant speed. The procedure (i)–(iv) is justified for two reasons: first, the time constant involved in the establishment of the shear flow turns out to be large compared to the duration of the experiment (a few minutes compared to 20 s); therefore, in order to keep the shear as steady as possible, the rotation of the disks is maintained constant. Secondly, it is preferable to investigate the phenomenon in the absence of body forces for the sake of comparison between theory and experiment; this condition imposes the quenching of the current and the restriction on the decay period.

Owing to the presence of friction at the bottom, the vorticity of the vortex decreases during the decay phase, while the shear remains fixed. Therefore we need to correct for this effect when we calculate the ratio between the maximum vorticity in the vortex core and the shear, which is an important parameter of the system. We shall return to this question below.

The two-dimensionality of the flow is also an important issue. We have checked, by studying elementary and well-documented situations (dipole propagation, merging of like-signed vortices, dipole collision, dipole propagating against a wall), that the behaviour of the system is similar to that of two-dimensional flow. We recently performed detailed velocity measurements simultaneously in the inner layer and on the free surface, for a decaying vortex and a propagating dipole (Paret *et al.* 1996); these experiments allow the flow structure within the layer to be analysed. We found that
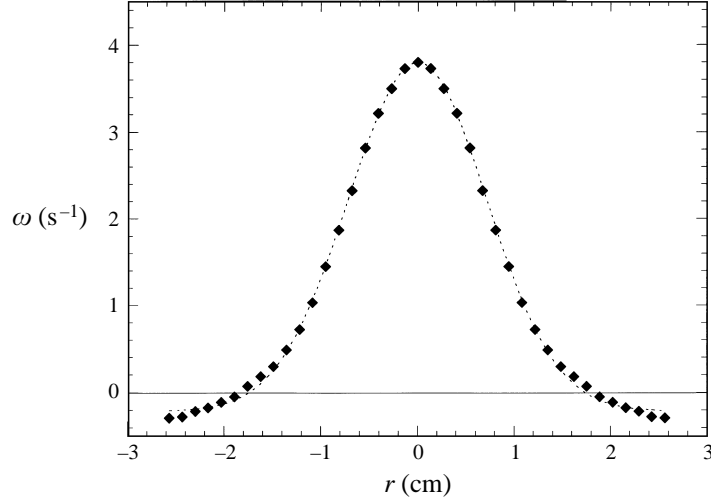
FIGURE 2. Typical vorticity profile of a vortex created in the absence of an external flow. This radial profile integrated on a circle is taken at $t = 0$. A Gaussian curve fitting the profile of the vortex is plotted.

after a transient regime (1–2 s), momentum is transferred throughout the fluid layer. Beyond this regime, the flow occurs both in the lower and upper layers. The relaxation of the three-dimensional effects is due to the presence of stratification. Moreover, Jüttner *et al.* (1997) have done a quantitative comparison between direct numerical simulation of two-dimensional Navier–Stokes equations and experiments for the particular problem of free turbulent decay. A good agreement is found between two-dimensional direct numerical simulation and the experiment. These results support the conclusion that the flow can be considered as two-dimensional in the experiment.

2.2. *Characterization of the single vortex* (*without an external shear*)

Figure 2 shows the vorticity profile of the single vortex generated according to the experimental procedure described above. The profile is produced without an external shear by imposing an electric current $I = 1.5$ A for a duration $\tau = 1.5$ s. We have used the same excitation parameters throughout all the experiments. The profile is shown at $t = 0$. The maximum vorticity ω_{max} at the vortex core is 3.8 s^{-1}, and the radius – determined by considering the contour where the velocity is maximum – is $r = 1.2$ cm. This corresponds to a vorticity level $\omega = 0.3\omega_{max}$. One also sees a ring of weak negative vorticity around the vortex. The amplitude of the negative ring corresponds to 4% of the positive vorticity part and we assume that it can be neglected. The Reynolds number can be defined as $Re = \omega_0 r^2/\nu$, where ν is the kinematic viscosity and $\omega_0 = \omega_{max}(t = 0)$. We find a value of Re of about 600. In the absence of shear, the structure and the size of the vortex remain constant during the decay phase while the energy and the maximum vorticity decrease exponentially with time. The evolution of the maximum vorticity is shown in figure 3. The exponential decrease is characterized by a time constant of 20 s; this value is consistent with the estimate $4b^2/\pi^2\nu$ (giving 25 s), which is obtained by decomposing the velocity profile, within the fluid layer, into Fourier series, resolving the Stokes equation, and tracking the evolution of the dominant Fourier mode. A convenient way to correct for the effect of the bottom friction is to plot the maximum ω^*_{max} of the compensated vorticity defined as

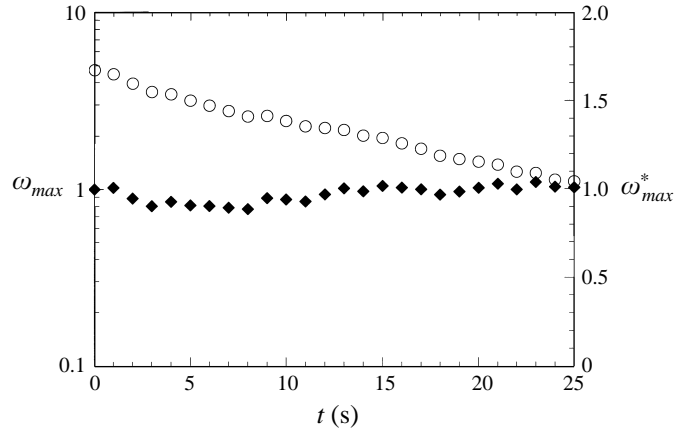$$\omega^*(\boldsymbol{x}, t) = (\omega(\boldsymbol{x}, t)/\omega_0) \exp(t/\tau_\nu). \tag{2.3}$$

FIGURE 3. Maximum of vorticity ω_{max} (circles) and compensated maximum of vorticity $\omega^*_{max}(t) = (\omega_{max}/\omega_0)\exp(t/\tau_\nu)$ (diamonds), as a function of time, for a single vortex, without external shear.
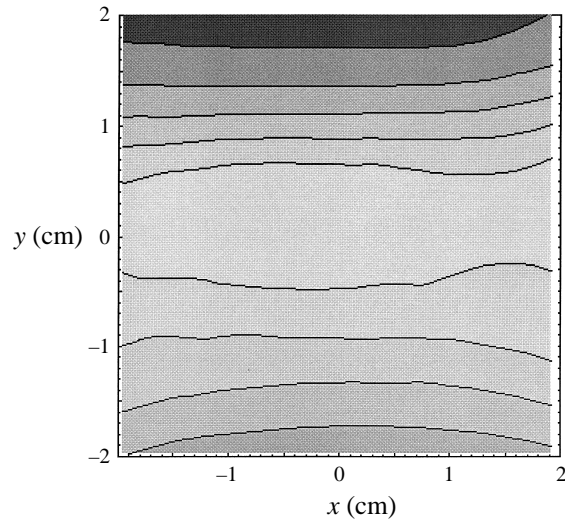

FIGURE 4. Streamlines of the external shear in the region between the two disks where the vortex is localized. The horizontal directions of the external shear x and y are respectively perpendicular and parallel to the axis joining the centres of the disks. The extremal streamfunctions ψ are: $\psi_{min} = -0.30$ cm^2 s^{-1} and $\psi_{max} = 0.35$ cm^2 s^{-1}.

Figure 3 shows that ω^*_{max} is indeed constant during the decay phase. The advantage of considering the compensated vorticity rather than the actual one is that it is easier to identify situations where the maximum vorticity decreases at a rate larger than due to viscosity alone.

2.3. Characterization of the shear flow

The streamlines of the flow produced in the upper layer by the two rotating disks are shown on figure 4. This pattern is obtained 7 min after the onset of rotation. Just after the onset, there are large velocity gradients close to the disks, and no flow in the central region. Then gradients are reduced and the flow is established between the disks, over a period of a few minutes, under the action of diffusion. The shear is stable for rotation rates smaller than 70 mHz. At larger rotation speeds, instabilities become visible after
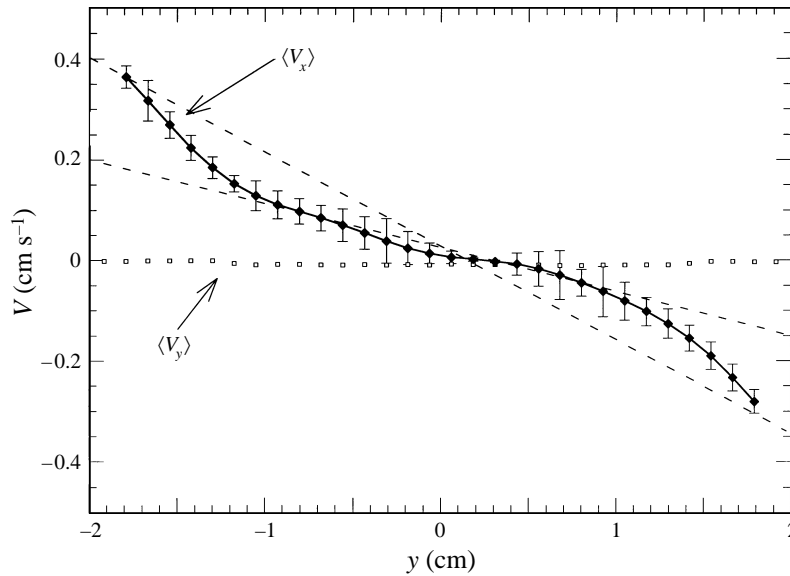
FIGURE 5. Profile of the imposed external velocity field. The two dashed lines represent the corresponding limiting slopes. Error bars indicate the standard deviation for each point.

10 min. We presume that this is an inflexional instability, but we have not analysed it in detail. We therefore can define a window within which the shear can be considered as established and remaining stable. This window is, in the worst case between 6 and 10 min. We shall see that this period of time is comfortably larger than the duration of an experiment. This suggests that there is no coupling between the phenomenon we study and the modes of instability of the shear. We have used, throughout the experiment, the same conditions for the establishment of the shear: the vortex is produced 7 min after the onset of the rotation. The limited size of the window in the time domain must be viewed as a significant experimental constraint.

The average profiles of the two components of the velocity field are shown on figure 5, along an axis joining the centres of the disks, again 7 min after the onset of rotation. The average is taken over a period of 18 s across the region where the vortex is generated. As expected from the symmetry of the device, the velocity V_y parallel to the axis is negligible within the accuracy of the measurements. This property holds in a region several cm wide between the disks. As shown by the error bars corresponding to one standard deviation, the perpendicular velocity is estimated with a good accuracy. It vanishes at the centre of the interval where it exhibits an inflexion point. The local strain $s = \frac{1}{2}\delta V_x/\delta y$ varies significantly within the interval. The value in the central region $s_1 = 0.045$ s^{-1}, taken between $y = -1.2$ cm and $y = 1.2$ cm, is shown as the initially lower of the two dashed lines on figure 5. The initially upper dashed line is drawn between the two extreme points of the curve at $y = \pm 1.8$ cm located where the vorticity equals zero (see figure 2). The corresponding strain is $s_2 = 0.09$ s^{-1}. The mean strain $S = 0.07$ s^{-1} is defined by taking the average of the two estimates s_1 and s_2.

The experimental design allows one to work with cooperative or adverse shears (i.e. with vorticity of the same or opposite sign to the vortex). In the case of a cooperative shear, we observe that the vortex remains essentially unaffected by the shear, which is not surprising according to the theoretical studies of Kida (1981) and Dritschel (1989). The cooperative shear is expected to produce a less dramatic effect on the vortex since equilibria exist for vorticity patches for any value of the strain. We thus focus in this

paper on the adverse case which displays more interesting dynamics. All the experiments presented here have been performed for the case of adverse shear.

2.4. *Definition of the control parameters of the experiment*

At any given time, an isolated vortex subjected to an external shear S is characterized by its maximum vorticity ω_{max}, the ratio $\gamma = S/\omega_{max}$ and the Reynolds number Re. In our experiment, ω_{max}, γ, and Re are varying parameters, since the vortex decays with time owing to the friction of the fluid against the bottom wall, as explained in §2.2. In order to measure the effect of the external shear, and to isolate it from friction effects, we use the compensated maximum vorticity defined by (2.3). Applying the same normalization, we define a compensated strain-to-vorticity ratio $\hat{\gamma} = (S/\omega_0)\exp(t/\tau_\nu)$ and a compensated Reynolds number $\widehat{Re} = (\omega_0 r^2/\nu)\exp(-t/\tau_\nu)$ with $\tau_\nu = 20$ s. In all the experiments we have taken $\omega_0 = 4$ s^{-1}. The compensated strain $\hat{\gamma}$ increases by a factor 3 from the beginning to the end of an experiment. Conversely, $\widehat{Re}$ decreases with time but remains large (> 210) throughout the experiment.

Note that the eddy turnover time, which varies from about 0.8 s (π/ω_0) at the initial time to near 2.5 s at the end of the experiment, is small with respect to the viscous decay time. Therefore, it will be appropriate to discuss and interpret our results at any time as if $\hat{\gamma}$ and $\widehat{Re}$ were constant. In fact, the variation of the control parameter through the action of friction offers a convenient way to explore a substantial range of $\hat{\gamma}$ without complicating the analysis of the results, provided the quasi-stationarity hypothesis is used.

3. Results for an isolated vortex subjected to an adverse shear flow

3.1. *Results*

Figure 6 shows the evolution of a vortex subjected to an adverse shear flow. The vortex is visualized by fluorescein continuously injected in the core of the vortex, the cell being illuminated from above with black light. The dye is vertically injected from the bottom of the cell; because we form a jet to inject the dye, a radial velocity component appears and the streaklines are spiralling outwards (as seen on figure 6a). This phenomenon is thus intrinsic to the visualization technique, not to the vortex. The sequence of pictures illustrates a case where the evolution leads to total and fast break-up of the vortex. At the end of the excitation period ($t = 0$, figure 6a), the vortex core is roughly elliptic, but the exterior streaklines exhibit strong deformation. The second and third pictures (figures 6b, 6c) show the vortex being strongly elongated under the action of the shear and forming two arms expelled along the direction of the shear. In the fourth picture (figure 6d), the vortex is reduced to a thin patch which is rapidly torn apart. It is striking to observe that the vortex preserves an almost constant orientation during its breaking, which is at about 45° to the shear axis. During a fast decay this situation can easily be interpreted using the elliptical theory of Kida (1981): this orientation corresponds to a vanishing effect of the shear on the rotation of the vortex but to a maximum deformation effect. Therefore fast breaking during which the self-rotation of the vortex is negligible locks the vortex along this preferred orientation.

When the external shear is varied, two successive stages of the evolution of the vortex – erosion and breaking – emerge over the duration of our experiments. Figure 7 shows plots of the compensated vorticity $\omega^*(t)$ for different values of the shear and illustrates these different stages of the evolution of the vortex. On figure 7(a–c), which is obtained for $S = 0.061$ s^{-1}, the vortex is weakly affected throughout the duration $T = 20$ s of the experiment; in particular the core of the vortex remains intact and ω^*_{max} remains
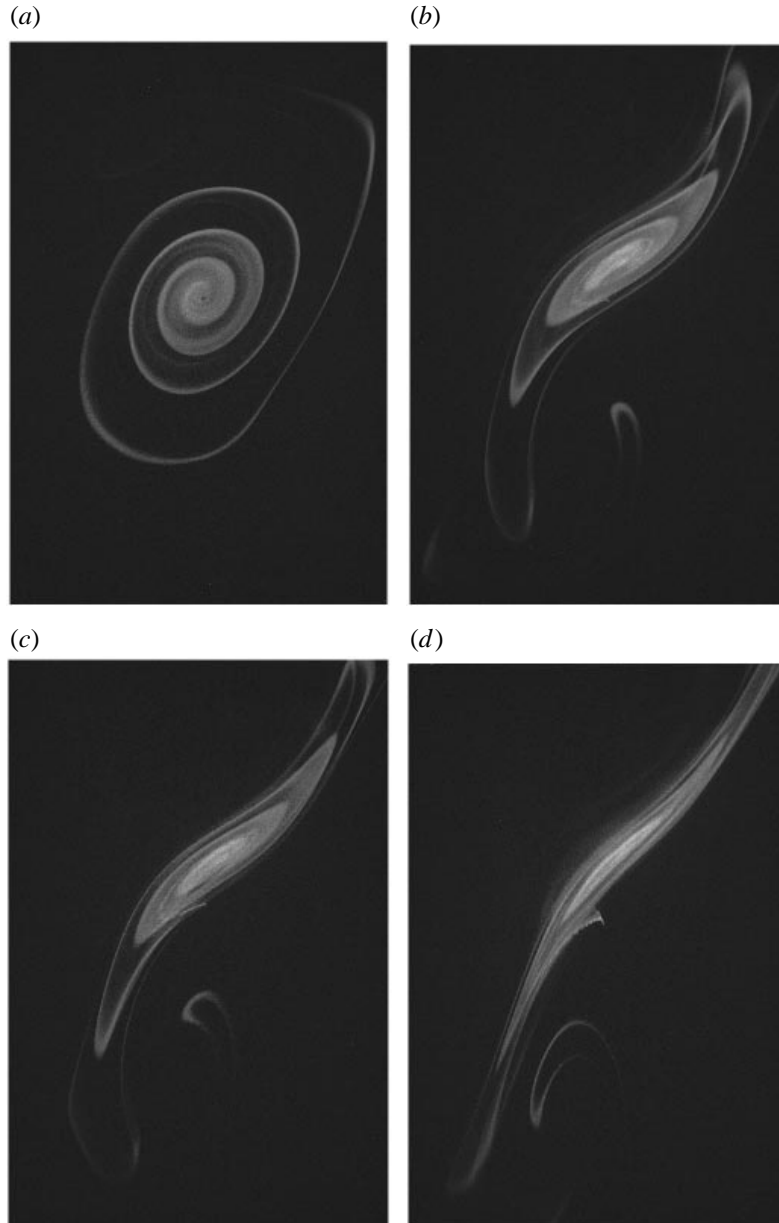
(*a*) (*b*)

(*c*) (*d*)

FIGURE 6. Evolution of a vortex visualized by fluorescein in black light) subjected to an adverse shear $S \approx 0.140$ s^{-1}. (*a*) $t = 0$, (*b*) $t = 4.4$ s, (*c*) $t = 7.2$ s, (*d*) $t = 8.4$ s. The dye is vertically and continuously injected during the experiment through a nozzle (1 mm) located on the bottom of the cell. The injection starts at $t = -\tau$. Because we form a jet to inject the dye, the streaklines are spiralling.

close to 1. The number of eddy turnover times, given by $(1/\pi)\int_0^T \omega_{max}\, \mathrm{d}t = (1/\pi)\,\omega_0\,\tau_\nu(1-\mathrm{e}^{-T/\tau_\nu})$, is approximately 15. Unlike the case without shear, the vortex does not retain its initial shape but is deformed and orientates itself perpendicularly to the shear. Using the theory of an elliptical vortex in a shear flow (Kida 1981), we may consider that this perpendicular orientation corresponds to a quasi-equilibrium position. While the vortex core is only elongated as an oval, there is evidence of erosion and expelling of the exterior layers of the vortex at the top and bottom of figures
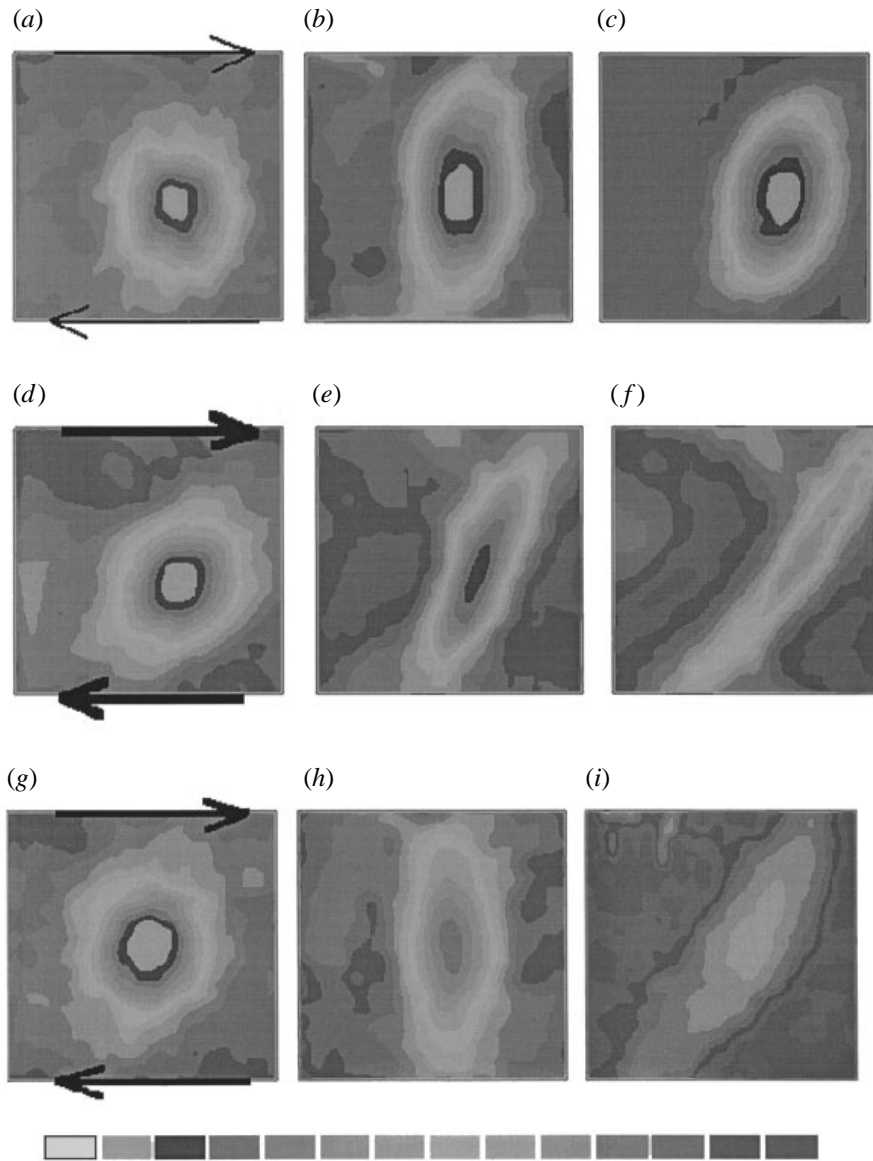
FIGURE 7. Evolution of the compensated vorticity field for a series of experiments using different shears. The size of the vorticity field is $(4.5 \times 4 \text{ cm}^2)$. The arrows indicate the direction of the shear. The grey-scale shows the vorticity levels (in s^{-1}). $(a–c)$ $S = 0.06 \text{ s}^{-1}$: (a) $t = 0$, (b) $t = 5$ s, (c) $t = 16$ s; $(d–f)$ $S = 0.155 \text{ s}^{-1}$: (d) $t = 0$, (e) $t = 3$ s, (f) $t = 5$ s; $(g–i)$ $S = 0.093 \text{ s}^{-1}$: (g) $t = 0$, (h) $t = 6$ s, (i) $t = 18$ s.

$7(b)$ and $7(c)$. This erosion does not appear to significantly shorten the lifetime of the vortex, which is similar to that observed under pure friction in the absence of shear. Note that the ring of negative vorticity cannot be identified on figure $7(a-c)$.

In the presence of a strong shear (see figure $7d–f$), the erosion takes place only during a short period of time after which the vortex rapidly deviates from its equilibrium position and eventually breaks up (see figures $7f$). The pictures of figure $7(d–f)$, which are obtained for $S = 0.155 \text{ s}^{-1}$, span the different stages of the breaking process. The vortex is now immediately stretched and the compensated maximum
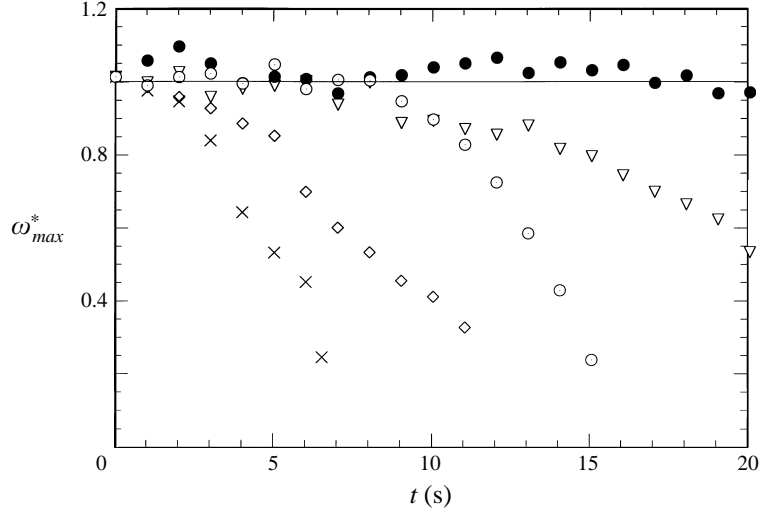
FIGURE 8. Evolution of the compensated maximum vorticity ω^*_{max} as a function of time for several experiments. ●, $S = 0.061$ s^{-1}; ▽, $S = 0.093$ s^{-1}; ⊙, $S = 0.129$ s^{-1}; ◇, $S = 0.135$ s^{-1}; ×, $S = 0.155$ s^{-1}.

vorticity decays much more rapidly than for the weak shear case. The orientation is no longer perpendicular to the shear, the angle to the shear being 55° in figure 7(f). Note that the vortex is turned into a long thin patch of vorticity after 5 s, which corresponds to only five eddy turnover times; this indicates that breaking is fast compared to the erosion process.

For intermediate values of the shear, slow erosion and breaking are observed in sequence during the experiment. Figure 7(g–i) shows the compensated vorticity maps $\omega^*(t)$ for a case where $S = 0.093$ s^{-1}. We first recover the behaviour associated with the erosion process (figures 7a, b). The erosion takes place while the vortex remains perpendicular to the shear. During the second stage (figure 7i), the vortex changes its orientation and is rapidly torn apart. The evolution of the vortex under the action of the shear can thus be separated into two stages: the first corresponds to the deformation and the peeling of the external layers of the vortex while the core is preserved; the second corresponds to the stretching and breaking of the vortex accompanied by the fast decrease of the maximum of vorticity.

Figure 8 shows the evolution of ω^*_{max} as a function of time, for five experiments: those shown in figure 7 plus two other ones. As already noticed, ω^*_{max} remains almost constant throughout the erosion, which means that the actual ratio γ is close to $\hat{\gamma}$. In the cases of strong shear ($S = 0.135$ s^{-1} and $S = 0.155$ s^{-1}), ω^*_{max} decays rapidly from its initial value as a consequence of the rapid stretching of the vortex. The parameter $\hat{\gamma}$ then strongly underestimates the actual ratio 'felt' by the vortex.

As shown in figure 8, for $S = 0.093$ and 0.129 s^{-1}, ω^*_{max} remains roughly constant for a period of time, and then decreases abruptly. A critical time t_c can be defined as the time characterizing the cross-over between these two regimes. To give orders of magnitudes, for $S = 0.129$ s^{-1}, t_c is approximately 8 s while for $S = 0.135$ and 0.155 s^{-1}, t_c is estimated as 4 s and 2 s respectively. This provides a simple way to define break-up onset; however, since the decay of ω^*_{max} requires the action of viscosity, one may suspect that it is somewhat delayed after the onset of breaking. In order to provide a more accurate estimate of the separation between the two stages of the vortex evolution, we have measured the temporal evolution of the orientation of the vortex.
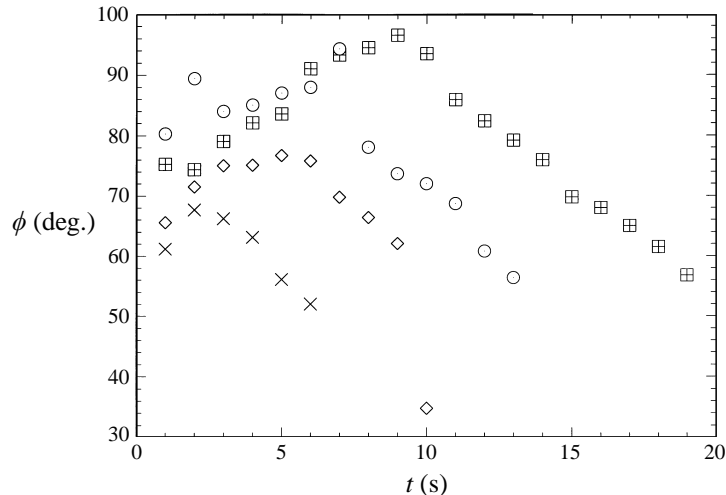
FIGURE 9. Temporal evolution of the vortex orientation ϕ for several experiments.
$\boxplus$, $S = 0.093$ s^{-1}; $\odot$, $S = 0.129$ s^{-1}; $\diamond$, $S = 0.135$ s^{-1}; $\times$, $S = 0.155$ s^{-1}.

Figure 9 shows the evolution of ϕ, the angle of the vortex to the direction of the shear. As the vortex is created in the presence of the shear, ϕ fluctuates and increases during the first few seconds in all experiments. For $S = 0.129$ and 0.093 s^{-1}, ϕ approaches and overshoots the equilibrium position – which corresponds here to an orientation of $90°$ – and, after that, suddenly decreases. For $S = 0.135$ and 0.155 s^{-1} the vortex does not reach an equilibrium but the abrupt decrease of ϕ is still observed. This sudden change of orientation can be explained as the beginning of the breaking phase. It is known that, for a distributed vortex, breaking is preceded by a sudden rotation of the vortex towards the axis of extensional strain. During the final step of the erosion, ϕ rapidly decreases until the total breaking of the vortex. Notice that an orientation of the vortex at $45°$ corresponds to a position of maximum deformation effect. We considered the different instants t_ϕ where ϕ decreases and compared them with the critical times t_c previously determined from figure 8: in all the experiments, the times t_ϕ we get are quite close to the critical times t_c defined previously.

The temporal evolution of $A(t)/A_0$ where $A(t)$ is the area of the vortex and A_0 the area at $t = 0$, is reported in figure 10. This quantity is obtained by fitting a particular contour of the vorticity map by an ellipse; in order to characterize the vortex core, the chosen level is such that $\omega^* = 0.3$ (see §2.2). The area A of this ellipse is then determined. In the case $S = 0.06$ s^{-1}, the area is conserved until $t \approx 5$ s, and then slightly decreases to $A/A_0 = 0.8$ at $t = 20$ s. This illustrates the weak erosion process which is observed in figure 7(a–c). For $S = 0.129$ s^{-1}, A/A_0 continuously decays throughout the experiment. Since the maximum compensated vorticity retains its initial value between $t = 0$ and 9 s (see figure 8), this stage is clearly an erosion of the vortex. Similarly, for $S = 0.093$ s^{-1}, A/A_0 is conserved until $t = 4$ s and decays afterwards while ω^*_{max} remains constant until $t = 12$ s. In the other experiments ($S = 0.135$ and 0.155 s^{-1}), characterized by early breaking, A/A_0 decreases abruptly as soon as the system is quenched. Notice that, for $S = 0.135$ s^{-1}, $\hat{\gamma}$ is increased by a factor 2 from $t = 0$ to 10 s while A/A_0 decreases practically from 1 to 0 over the same period. This illustrates that vortex breaking develops on a faster time scale than the one corresponding to the control parameter $\hat{\gamma}$, which somewhat justifies the assumption of quasi-stationarity made previously.
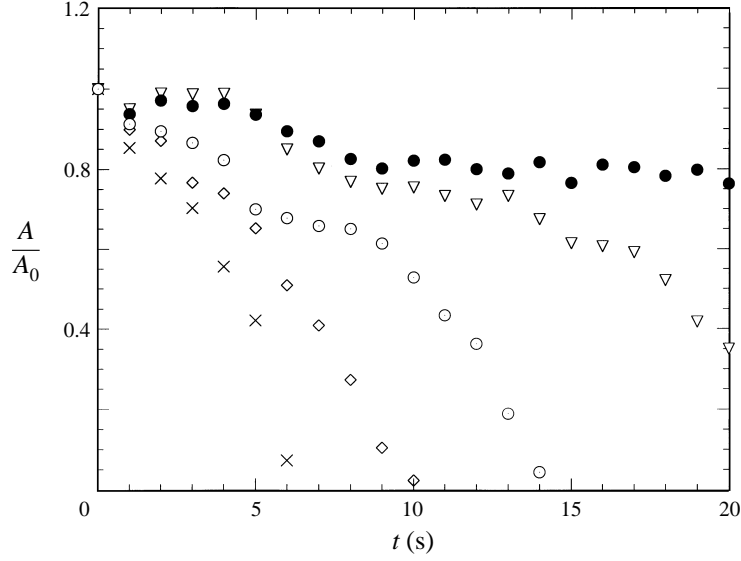
FIGURE 10. Temporal evolution of A/A_0 (the area A is divided by the initial area A_0) for the experiments of the previous figures. ●, $S = 0.061 \text{ s}^{-1}$; ▽, $S = 0.093 \text{ s}^{-1}$; ⊙, $S = 0.129 \text{ s}^{-1}$; ◇, $S = 0.135 \text{ s}^{-1}$; ×, $S = 0.155 \text{ s}^{-1}$.
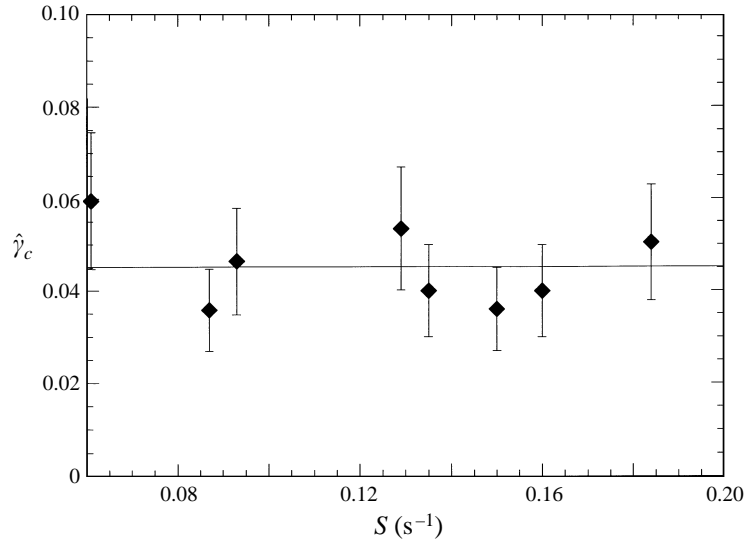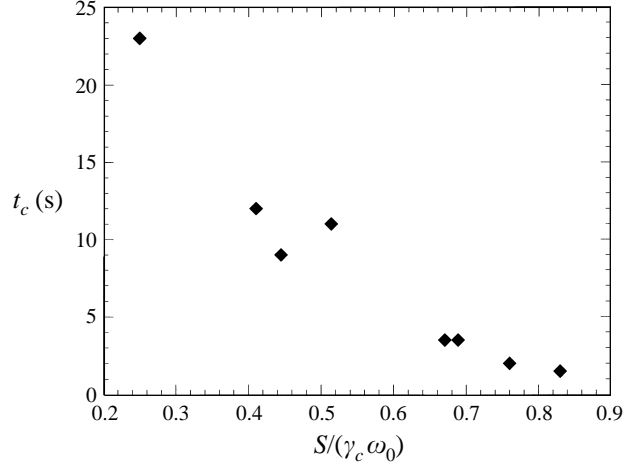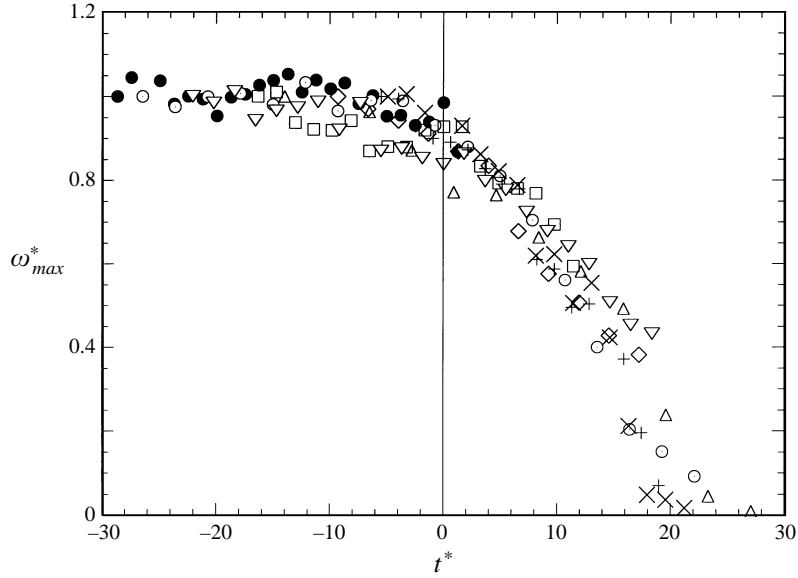

FIGURE 11. Critical value $\hat{\gamma}_c$ as a function of the imposed shear S. The error bars indicate the 25% deviation due to the estimate of S. The solid line indicates the mean experimental value $\hat{\gamma}_c = 0.045$.

3.2. *Critical parameters*

We shall now discuss the experimental values of the parameters defining the threshold between erosion and breaking. This threshold is associated with varying values of t_c: the larger the shear, the smaller t_c. However, the critical values of $\hat{\gamma}$ – denoted by $\hat{\gamma}_c$ – corresponding to the onset of breaking, when ω^*_{max} becomes smaller than 1, are the same for all the experiments. This is shown in figure 11, where we have plotted the critical value of $\hat{\gamma}$ as a function of the shear S. $\hat{\gamma}_c$ is constant within the error bars inferred from figure 5. The estimated value is $\hat{\gamma}_c = 0.045 \pm 0.011$. Assuming the

FIGURE 12. Critical time t_c as a function $S/\hat{\gamma}_c\omega_0$.

FIGURE 13. ω^*_{max} as a function of $t^* = (t-t_c)S/\hat{\gamma}_c$; $\bullet$, $S = 0.061$ s^{-1}; $\square$, $S = 0.087$ s^{-1}; $\triangledown$, $S = 0.093$ s^{-1}; $\odot$, $S = 0.129$ s^{-1}; $\diamond$, $S = 0.135$ s^{-1}; $+$, $S = 0.150$ s^{-1}; $\times$, $S = 0.155$ s^{-1}; $\triangle$, $S = 0.184$ s^{-1}.

existence of a critical value for $\hat{\gamma}$ one can deduce the expression for the critical time t_c and finds $t_c = -\tau_\nu \ln(S/\hat{\gamma}_c\omega_0)$. This shows that as S increases, t_c decreases, as shown in figure 12.

To compare with theory, it is appropriate to use the actual vorticity in the core of the vortex instead of the compensated vorticity. We have thus determined the value of $\gamma = S/\omega_{max}$ at time $t = t_c$. The mean value is $\gamma_c = 0.051 \pm 0.017$ which is larger than but close to $\hat{\gamma}_c$. The small difference is explained by the fact that ω_{max} remains close to $\omega_0 \exp(-t/\tau_\nu)$ during the erosion stage. Below, we shall compare this experimental value γ_c with the theory.

The decay phase for $t > t_c$ is of interest: we have found a way to collapse the set of curves of figure 8 onto a single one, by introducing the following variable: $t^* = (t-t_c)$

$S/\hat{\gamma}_c$. From the definition of $\hat{\gamma}$, the time $(\hat{\gamma}_c/S)$ is the turnover time of the vortex at $t = t_c$. There is some scatter, but the collapse can be considered as fairly good (figure 13). The universal curve can be roughly fitted, for $t^* \geqslant 0$, by a relation of the form $\omega^*_{max} = 2 - \exp(\alpha t^*)$ where $\alpha \approx 0.03$. This collapse may be considered surprising: it means that the time taken for the core vorticity to decrease to zero, under the action of a shear, depends only on S and $\hat{\gamma}$ and suggests that it depends only weakly on the fluid viscosity. This is in agreement with the results of Mariotti *et al.* (1994) who found that the fast exponential decay leading to complete destruction does not depends on *Re*. A first reason is that after $t = t_c$, the vortex soon becomes very thin, its width decaying exponentially with time. Therefore the dependence of ω^*_{max} on the Reynolds number is expected to be logarithmic at most. Also, before being dissipated by viscosity, the vortex becomes so thin that its core ceases to be spatially resolved by our analysis. The quantity which is measured is then a coarse-grained vorticity and it is no longer paradoxical to find that it decays on an inertial time scale.

4. Discussion and conclusion

It is worth commenting on the critical value of γ. The numerical value found for a continuous distribution of vorticity is $\gamma_c = 0.0675 \pm 0.0025$ (Mariotti *et al.* 1994). This value does not depend significantly on the particular vorticity distribution that is considered, and is independent of viscosity (provided the Reynolds number, based on the vortex size, is large). It is thus meaningful to compare this value to the experimental estimate we get, which is $\gamma_c = 0.051 \pm 0.017$. Taking into account the sizes of the error bars (which unfortunately are quite large), it is fair to say that the two estimates are consistent.

In conclusion, the present experiment shows excellent qualitative agreement with the theoretical expectations for the erosion and break-up processes. We also show the existence of a critical parameter governing the onset of break-up, as expected from the theory. On the quantitative level, the fact that the threshold values we get are consistent with the numerical findings reinforces the good correspondence between experiment and theory.

Finally, recall that one of the goals of the present study was to determine to what extent the theoretical approach and the numerical studies of an elementary process (e.g. a vortex subjected to a uniform shear in two dimensions) are realistic enough to interpret laboratory experiments. Our conclusion is that the theoretical framework applies well to the real world, both at qualitative and (to a lesser extent) quantitative levels. We thus propose that a complete, consistent, description of a particular phenomenon (vortex stripping and vortex break-up under the action of a shear), including theoretical, numerical and experimental approaches, is now available. This may be useful for analysing more complex situations, such as two-dimensional turbulence, where such a phenomenon is believed to play an important role.

REFERENCES

CARDOSO, O., MARTEAU, D. & TABELING, P. 1994 Quantitative experimental study of the free decay of quasi-two-dimensional turbulence. *Phys. Rev.* E **49**, 454–461.

DOLSZHANSKII, F. V., KRYMOV, V. A. & MANIN, D. YU. 1992 An advanced experimental investigation of quasi-two-dimensional shear flows. *J. Fluid. Mech.* **241**, 705–723.

DRITSCHEL, D. G. 1989 Strain-induced vortex stripping. In *Mathematical Aspects of the Vortex Dynamics* (ed. R. E. Caflisch), pp. 107–119. SIAM.

DRITSCHEL, D. G. 1990 The stability of elliptical vortices in an external straining flow. *J. Fluid. Mech.* **210**, 223–261.

GRIFFITHS, R. W. & HOPFINGER, E. J. 1986 Experiments with baroclinic vortex pairs in a rotating fluid. *J. Fluid. Mech.* **173**, 501–518.

HEIJST, G. J. F. VAN & FLOR, J. V. 1989 Dipole formation and collisions in a stratified fluid. *Nature* **340**, 212–214.

JÜTTNER, B., MARTEAU, D., TABELING, P. & THESS, A. 1997 Numerical simulations of experiments on quasi-two-dimensional turbulence. *Phys. Rev.* E **55**, 5479–5488.

KIDA, S. 1981 Motion of an elliptical vortex in a uniform shear flow. *J. Phys. Soc. Japan* **50**, 3517–3520.

LEGRAS, B. & DRITSCHEL, D. G. 1993 Vortex stripping and the generation of high vorticity gradients in two-dimensional flows. *Appl. Sci. Res.* **51**, 445–455.

LEGRAS, B. & DRITSCHEL, D. G. 1994 Vortex stripping. In *Modelling of Oceanic Vortices* (ed. G. J. F. van Heijst), pp. 51–59. North Holland.

MARIOTTI, A., LEGRAS, B. & DRITSCHEL, D. 1994 Vortex stripping and the erosion of coherent structures in two-dimensional flows. *Phys. Fluids* **6**, 3954–3962.

MOORE, D. & SAFFMAN, P. 1971 Structure of a line vortex in an imposed strain. In *Aircraft Wake Turbulence and its Detection* (ed. J. Olsen, A. Goldberg & N. Rogers) Plenum.

PARET, J., MARTEAU, D., PAIREAU, O. & TABELING, P. 1996 Are flow electromagnetically driven in thin stratified layers two-dimensional? *Phys. Fluids* (submitted).

TABELING, P., BURKHART, S., CARDOSO, O. & WILLAIME, H. 1991 Experimental study of freely decaying two dimensional turbulence. *Phys. Rev. Lett.* **67**, 3772–3774.

TRIELING, R. R. 1996 Two-dimensional vortices in strain and shear flows. PhD thesis, Eindhoven, The Netherlands.

VOROPAYEV, S. I. & AFANASYEV, Y. D. 1991 Two-dimensional vortex-dipole interactions in a stratified fluid. *J. Fluid. Mech.* **236**, 665–689.

WAUGH, D. W., PLUMB, R. A., ATKINSON, R. J., SCHOEBERL, M. R., LAIT, L. R., NEWMAN, P. A., LOWENSTEIN, M., TOOHEY, D. W., AVALLONE, L. M., WEBSTER, C. R. & MAY, R. D. 1994 Transport of the lower stratospheric Arctic vortex by Rossby wave breaking. *J. Geophys. Res.* **99**, 1071–1088.